ISSN 1029-9599, Physical Mesomechanics, 2018, Vol. 21, No. 5, pp. 464–474. © Pleiades Publishing, Ltd., 2018.
Original Russian Text © V.E. Panin, S.V. Panin, Yu.I. Pochivalov, A.S. Smirnova, A.V. Eremin, 2018, published in Fizicheskaya Mezomekhanika, 2018, Vol. 21, No. 4, pp. 33–44.

Structural Scale Levels of Plastic Deformation and Fracture of High-Strength Titanium Alloy Welds

V. E. Panin[1,2], S. V. Panin[1,2]*, Yu. I. Pochivalov[1], A. S. Smirnova[1], and A. V. Eremin[1,2]

[1] *Institute of Strength Physics and Materials Science, Siberian Branch, Russian Academy of Sciences, Tomsk, 634055 Russia*
[2] *National Research Tomsk Polytechnic University, Tomsk, 634050 Russia*
** e-mail: svp@ispms.tsc.ru*

Received July 10, 2018

Abstract—Structural scale levels of plastic deformation and fracture of welded joints have been studied for two high-strength titanium alloys with a low (VT18U alloy) and a high (VT23 alloy) content of the bcc β phase. Ultrasonic forging and its combination with high-current pulsed electron beam treatment were used to activate nanoscale structural levels of deformation and fracture in welds in order to increase the fatigue life of welded structures. Ultrasonic forging provides an effective dispersion and nanostructuring of surface layers in the VT18U welded joints with a 4.6-fold increase in their fatigue life. The dispersion and nanostructuring of the VT23 laser welded joints is achieved only by ultrasonic forging combined with high-current electric pulse treatment, in which longitudinal dispersion of β bands occurs with the formation of orthorhombic α″ nanolaths. In so doing, the fatigue life of the VT23 welds increases twice, but the effect depends on the power of the high-current generator and electrical pulse parameters. The fracture micrographs of the treated VT23 welded joints reveal nanofibrous bands responsible for ductile fracture and for the reduction of the fatigue crack growth rate. The structural changes and the increase in the fatigue life of the studied titanium alloy welds are associated with the activation of nanoscale structural levels of deformation and fracture induced by ultrasonic forging or by its combination with high-current pulsed electron beam treatment.

DOI: 10.1134/S1029959918050107

Keywords: titanium alloys, welded joints, structural scale levels, plastic deformation, fracture, fatigue life

1. INTRODUCTION

Conventionally, plastic deformation and fracture of solids are described under the assumption that the initial crystal lattice of a deformed solid is translation-invariant. This methodological basis also underlies the theory of deformation defects in the physics of plasticity and strength of materials.

The crystalline structure of the weld material has broken translation invariance due to welding processes. In addition, the welded joint is very different in structure and composition from the base material. Its structure is highly heterogeneous at the macroscale and has high lattice curvature. The structurally heterogeneous medium is characterized by a specific electron energy spectrum that is poorly conjugated with the electron subsystems of welded metals. Therefore, the main role under loading of the medium belongs to higher structural scale levels of deformation. For this reason, the plastic deformation of the welded joint cannot occur concurrently with that of the adjacent heat affected zones, due to which mesoscopic localized shear bands propagate from the weld to these (conjugate) zones with their subsequent cracking [1].

As for the welded joints of complex alloyed steels and alloys, complex intermetallic and chemical compounds can be formed in heat affected zones even in the absence of melting and crystallization in these zones. Like in the weld material, plastic deformation in heat affected zones cannot occur together with that of the translation-invariant base material under mechanical loading. That is why the macro- and microstructure of the weld and heat affected zones must be dispersed.

An effective way to achieve the strength properties of the welded joint close to the base metal ones is to control the structural scale levels of plastic deformation and fracture in different zones of the weld [2].

The aim of this paper is to study the structural scale levels of plastic deformation and fracture in welded joints of high-strength titanium alloys VT18U and VT23, which have a different content of the high-strength bcc β phase, and to increase their fatigue life by activating mesoscopic structural states at lower scale levels.

The alloy VT18U has the composition Ti–6.5Al–4Zr–3Sn–1Nb–0.7Mo–0.2Si and only 2–3% of the high-strength β phase. We propose to use ultrasonic forging to disperse the bcc β phase in this alloy and to activate mesoscopic structural states at the micro- and nanolevels. We assume that ultrasonic forging is accompanied, in addition to the dispersion of the high-strength β phase, by the development of lattice curvature, which triggers the motion of point defects at the microlevel [3, 4]. This should be favorable for the increase in the fatigue life of the VT18U welded joints, despite the fact that they are produced by semi-automatic argon arc welding.

The alloy VT23 has a more complex composition Ti–5Al–4.5V–2Mo–1Cr–0.7Fe, and its laser welded joints have very low ductility. It is known that the β-phase dispersion is difficult to achieve by ultrasonic forging at a high concentration of the β phase that contains V, Mo, and Cr with strong covalent d bonds. We propose to combine ultrasonic forging with high-current electric pulse treatment [5], which can cause splitting of β-phase bands with the growth of α″ laths in them. This can weaken covalent bonds in bundles of β-phase bands and activate mesoscopic structural states at numerous interfaces between the α″ and β phases. Similar effects were observed under high-temperature superplastic deformation of Ti_3Al-based titanium alloys [6]. The effect of ultrasonic forging combined with high-current pulsed electron beam treatment on titanium alloy welded joints is studied for the first time in this paper.

2. MATERIALS AND EXPERIMENTAL PROCEDURE

Materials for the investigation were weldable high-strength titanium alloys VT18U (Ti–6.5Al–4Zr–3Sn–1Nb–0.7Mo–0.2Si) and VT23 (Ti–5Al–4.5V–2Mo–1Cr–0.7Fe). Welded joints of the pseudo-α titanium alloy VT18U were produced by semi-automatic argon arc welding. The argon arc welding of 3mm thick sheets was carried out on an ADSV-7 welding machine with direct current straight polarity. Welded joints of the (α + β) titanium alloy VT23 were laser welded with a CO_2 laser using argon and helium shielding gases. Laser welding was carried out on a SIBIR welding system developed at the Institute of Theoretical and Applied Mechanics SB RAS (Novosibirsk). The laser power was 3 kW; the welding speed $V_w \sim 15$ mm/s.

Metallographic examination was performed on a Stemi 2000-C stereomicroscope and an Axiovert 25 CA optical microscope. Etching of thin sections was carried out in a 2% aqueous solution of hydrofluoric (HF) acid and nitric acid (HNO_3). Electron microscopy studies of a thin surface layer were performed using a JEOL-2100 and JEM 100 CXII transmission electron microscopes. Thin foils for the study were prepared by standard techniques.

Mechanical tests were performed in accordance with GOST 1497-84 and GOST 6996-66 by static tension on an Instron-5582 universal electromechanical testing machine. Fatigue tests were carried out on a Schenck Sinus 100.40 and 15 kN BISS Nano servohydraulic testing machines according to GOST 7855-84, with an asymmetric loading cycle ($R = 0.1$).

Fractographic examination of specimens after low-cycle fatigue tests was carried out with a Tesla BS-300 scanning electron microscope equipped with a digital image acquisition system.

Ultrasonic forging of the surface layers of specimens was carried out using an IL4 ultrasonic generator designed to generate a current of 25 kHz with an up to 630 W power output, and a working tool that converts electrical oscillations into mechanical vibrations (magnetostrictive ultrasonic transducer).

The laser welded joints of titanium alloy VT23 were additionally subjected to ultrasonic forging combined with high-current electric pulse treatment. The pulse duration τ was 10 μs; the voltage applied to the metal surface was 50 V; and the pulse repetition frequency was 1000 Hz.

Since the laser welded VT23 specimens with permanent joints exhibit a complex fatigue fracture behavior, the digital image correlation method was used to quantitatively determine the fatigue crack initiation and growth parameters to analyze deformation behavior under cyclic tension.

Flat specimens with the gage section dimensions $50 \times 10 \times 2$ mm^3 had a weld in the central part. The cyclic loading of the specimens was carried out on a Biss UTM 150 servohydraulic testing machine with the following parameters: the maximum load in the cycle $P_{max} = 9$ kN (which is $\sigma = 500$ MPa, or $0.45\sigma_B$); and the cycle asymmetry $R = 0.1$. Such loading parameters were chosen to simulate low-cycle fatigue conditions with the number of cycles not exceeding $N = 5 \times 10^4$ cycles. Digital image

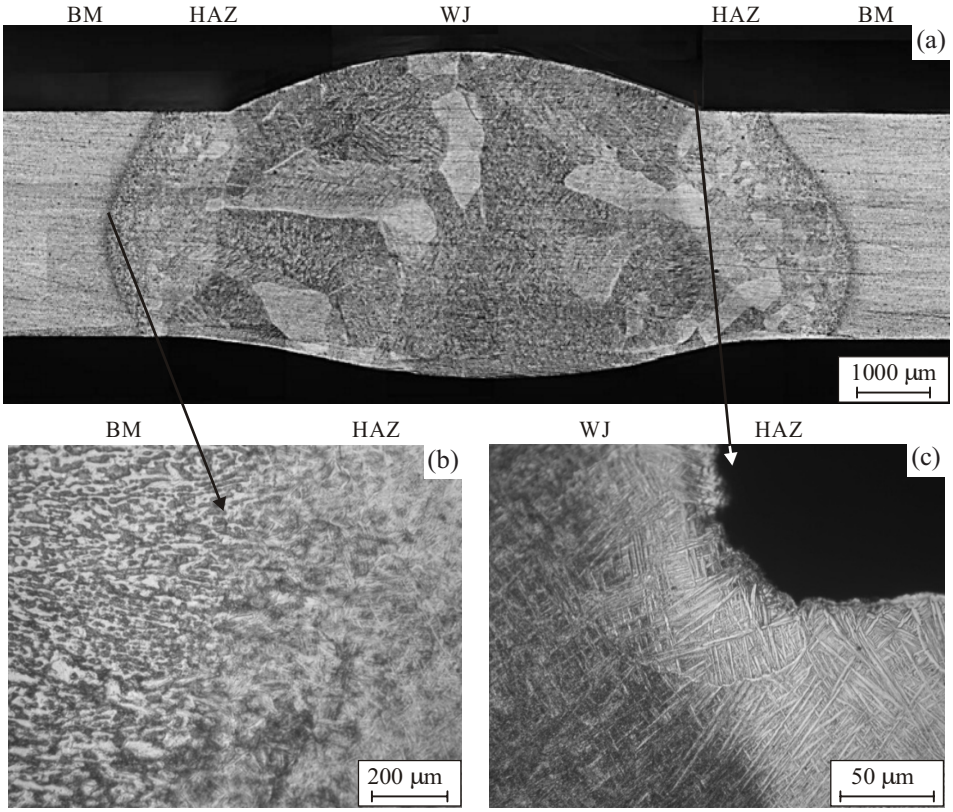

Fig. 1. Structure of VT18U titanium alloy weld: panoramic view of the welded joint (a); transition zone between base metal (BM) and heat affected zone (HAZ) (b); transition zone between welded joint (WJ) and heat affected zone (HAZ) (c).

correlation was used to observe the crack propagation path directly during the test.

Cracks can initiate on both flat faces of a welded specimen under cyclic loading. For this reason, the test specimen was photographed from two sides using Canon EOS 700D digital cameras equipped with Canon EF 70–300 mm/4.0-5.6L lenses. The magnification during photography was 5 μm/pixel, such that the entire specimen length and width were observed. The surface was photographed every $\Delta N = 500$ cycles with loading paused at the maximum tensile stress ($\sigma = 500$ MPa). Software VIC-2D 2009 (Correlated Solutions Inc., USA) was used to calculate displacement fields, strains, and crack growth parameters.

3. INVESTIGATION RESULTS

3.1. Structural Scale Levels of Plastic Deformation and Fracture of VT18U Alloy Welds

The general view of the VT18U welded joint is shown in Fig. 1. During cyclic deformation, a stress concentrator appears at the weld root boundary and gives rise to a fatigue crack that rapidly propagates through the 2 mm thick specimen. The weld fatigue life does not exceed $N = 24\,400$ cycles. It was necessary to induce deformation at lower scale levels in the VT18U weld, which was done by ultrasonic forging that modified the weld structure.

Figure 2 shows TEM micrographs of the VT18U weld structure before and after ultrasonic forging. The welded joint with the initial structure reveals numerous bands of different origin (β phase, α′ phase, etc.) (Fig. 2a), while after ultrasonic forging the material becomes nanostructured (Figs. 2b and 2c). This is well illustrated by circular reflections in the microdiffraction pattern (Fig. 2b) and by a wide range of nanoparticle sizes in the dark-field image of the microstructure. Since the crystalline structure of the nanoparticle boundaries is unstable to shear, stress concentrators are not formed at the weld root boundary.

A fatigue crack in a cyclically loaded nanostructured weld is always initiated on the lateral face of the specimen and propagates across the entire width of nanostructured material. In so doing, the fatigue life of the nanostructured VT18U welded joint increased more than 4.6 times and reached $N = 150\,000$ cycles.

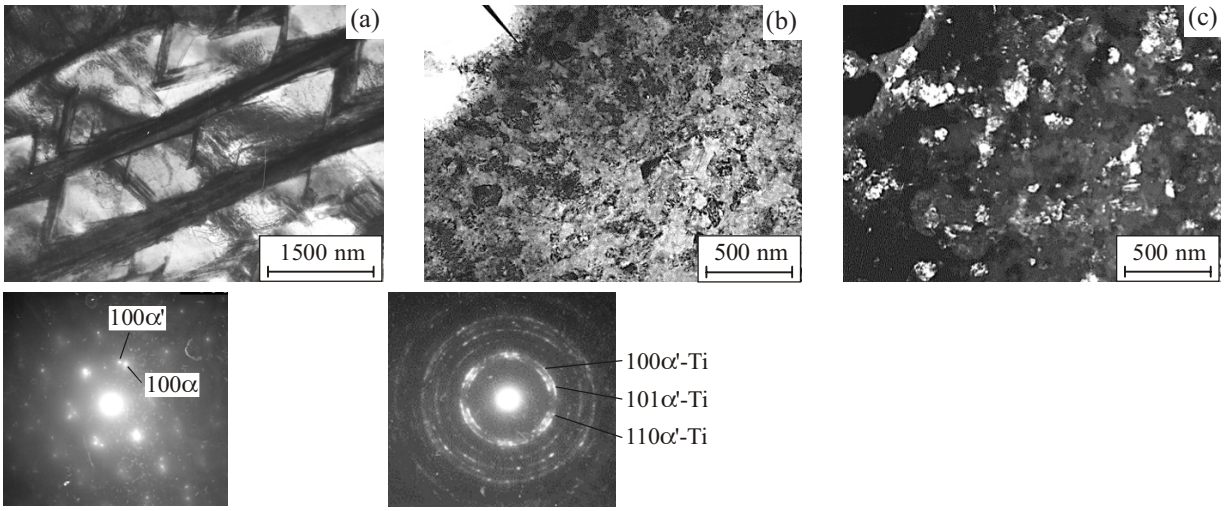

Fig. 2. TEM image of VT18U alloy weld structure in the initial state (a), after ultrasonic forging in the bright field (b), in the dark field of the α′-Ti reflection (c).

It should be noted that ultrasonic forging of weld surface layers causes their plastic deformation in conjugation with an elastically loaded underlying material, and gives rise to residual compressive stresses in the surface layer (up to $\sigma_p = 127 \pm 51$ MPa) instead of residual tensile stresses ($\sigma_s = 64 \pm 21$ MPa) in the unforged weld material. This factor also contributes to increasing the fatigue life of the permanent joint. However, the major effect of surface layer nanostructuring on the weld fatigue life is the dispersion of the sharp interface between the weld root and the surrounding material, where concentrated stresses relax during ultrasonic forging and cyclic loading. The deformation of shear-unstable boundaries in nanostructured material is responsible for the activation of the nanoscale structural level of deformation, which is the most effective factor of relaxation affecting the initiation and growth of fatigue cracks. This is even more evident in VT23 alloy welds processed by ultrasonic forging in combination with high-current electric pulse treatment.

3.2. Structural Scale Levels of Plastic Deformation and Fracture of VT23 Alloy Welds

The microstructure of the VT23 welded joint is represented by globular α-phase particles of size 2–4 μm located along the grain boundaries of β-phase particles of size 3–8 μm. The processing of such welded joints by ultrasonic forging does not change their strength and ductility, as well as does not increase their fatigue life.

A combination of ultrasonic forging with high-current electric pulse treatment leads to structure refinement in coarse grains with the formation of a fine-grained banded structure. Thin martensitic α′ laths are formed in the α phase, and thin α″ laths of thickness 10–20 nm appear in the β phase. Dark-field analysis shows that the misorientation of the banded structures does not exceed 10°–15°. Low-cycle fatigue tests showed that after the complex processing by ultrasonic forging with electric pulse treatment the number of cycles to fracture increased to $N = 58\,700$, which is twice the fatigue life of the untreated welds. There is reason to believe that the fatigue life of the VT23 welded joint can be significantly increased with increasing power of applied high-current pulses.

X-ray diffraction study revealed that the β-phase peak intensity decreases in the welded joint after combined treatment (Fig. 3). This is indicative of a decrease in the amount of the β phase due to its transformation into nanostructured α″ laths. The peak broadening indicates a decrease in the size of all grain structure elements during the growth of α′-martensite laths in the α phase and α″-martensite laths in the β phase.

TEM micrographs in Fig. 4 demonstrate the VT23 weld structure in the initial state and after ultrasonic forging combined with high-current electric pulse treatment. As can be seen from Fig. 4c, the complex treatment causes splitting of the β-phase bands across the entire weld thickness. This testifies to the high relaxation ability of VT23 welded joints due to nanostructuring of their initial structure by the combined treatment. Such a structure is formed as a result of atomic rearrangements at nanostructural levels of deformation, which are activated

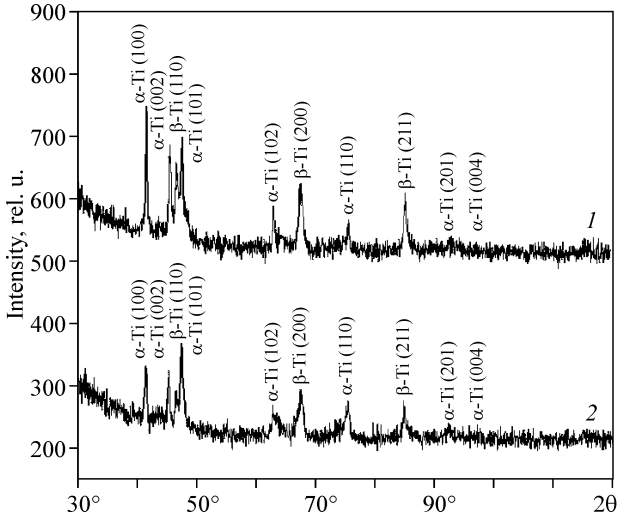

Fig. 3. X-ray diffraction pattern of VT23 titanium alloy weld, laser welding: *1*—unforged weld; *2*—weld after ultrasonic forging with high-current pulsed electron beam treatment.

in the material during the combined treatment. This effect is even more clearly observed with the initiation and growth of fatigue cracks in the fracture patterns.

3.3. Structural Scale Levels of Fracture of VT23 Alloy Welds in Different Structural States

The VT18U alloy welds were processed only by ultrasonic forging that gives rise to lattice curvature, plastic distortion, and increases the role of the motion of point defects in plastic deformation and fracture. More structural scale levels of deformation and fracture are activated in the VT23 alloy weld under ultrasonic forging combined with high-current electric pulse treatment. In so doing, structural phase transformations of the α and β phases take place under plastic deformation and fracture in the conditions of material nanostructuring. Let us consider these processes in more detail.

Figure 5 shows SEM fracture micrographs of the VT23 welded joints obtained after low-cycle fatigue tests of unforged specimens and specimens subjected to ultrasonic forging combined with high-current electric pulse treatment. In all cases, the crack is initiated from the lateral face of the specimen and then propagates across the specimen through its entire width. However, the fracture surface profiles in the initial specimens and after the combined treatment differ greatly. The fatigue

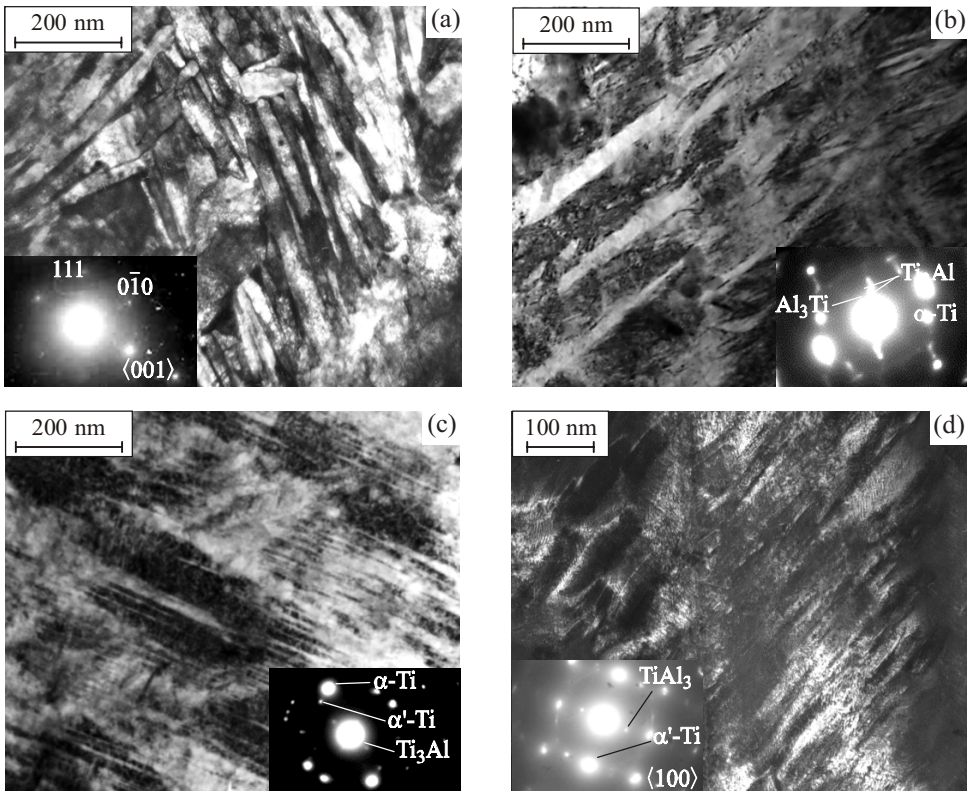

Fig. 4. Fine-grained structure formation in a thin surface layer of VT23 laser weld as a result of ultrasonic forging combined with electric pulse treatment: base metal VT23 (a); weld zone (b); weld zone after combined treatment (c); dark-field image of the weld zone subjected to combined treatment in the α″-phase reflection (d).

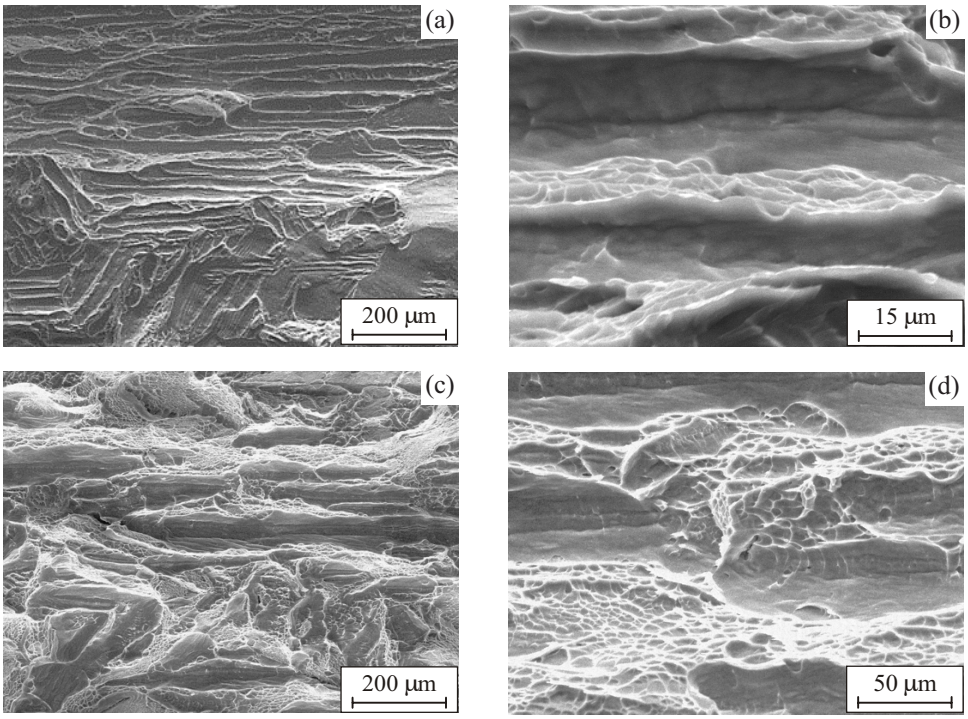

Fig. 5. SEM fracture micrographs of VT23 laser weld. Low-cycle fatigue. Untreated weld: fibrous banded surface relief in the zone of accelerated crack growth (a), magnified image (b). After ultrasonic forging with electric pulse treatment: fibrous banded surface relief with a large component of ductile rotation in the relief (c), magnified image (d).

crack forms transverse river-like grooves on the fracture surface of the unforged weld and thus produces narrow ductile fracture zones. After the combined treatment the width of ductile fracture zones sharply increases (Figs. 5c and 5d), while the width of cleavage zones decreases drastically. The ductile fracture zones exhibit dynamic rotations of the plastic flow with the formation of a nanofibrous structure. As a consequence, the fatigue life of the VT23 alloy welds increases more than twofold.

Naturally, the fatigue crack growth rate should decrease with increasing fracture toughness. This effect was verified in special experiments. The process of fatigue crack initiation and growth was observed by photographing both surfaces of welded joints with subsequent image processing by digital image correlation using Vic-2D software.

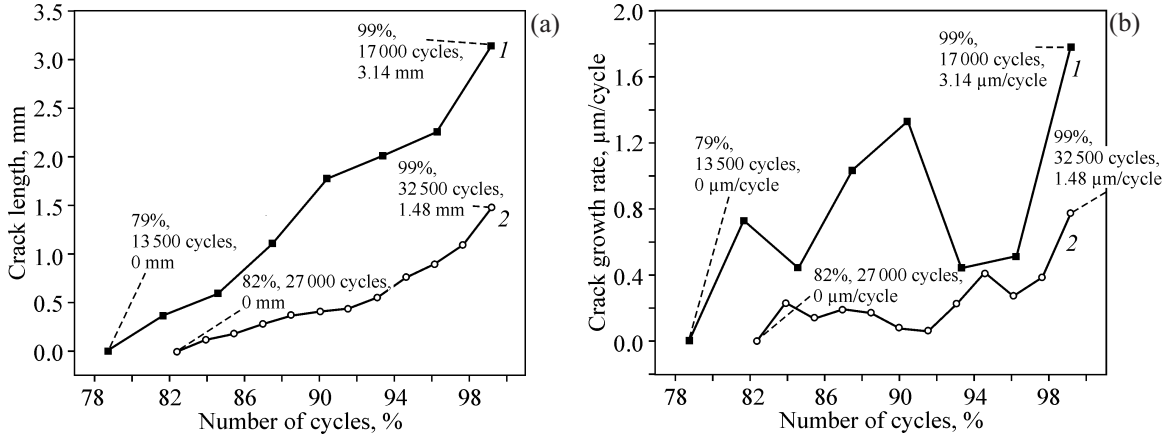

Fig. 6. Crack length (a) and crack growth rate (b) versus normalized number of cycles to fracture for the welded joint in the initial state and after ultrasonic forging combined with pulsed electron beam treatment.

3.4. Digital Image Correlation Analysis of Specimen Deformation Behavior

By analyzing the obtained images of flat faces of a cyclically deformed specimen, we estimated the length of the crack that reaches the specimen surface and the crack growth rate (Fig. 6).

Signs of crack initiation in the images of strain fields ε_1 are visually observed as local inhomogeneities; they are detected at $N = 11\,000$ cycles for the unforged specimen, and at $N = 12\,000$ cycles for the specimen subjected to ultrasonic forging with high-current pulsed treatment. A visually observed crack appears on the surface at $N = 14\,000$ cycles in the first case, while after combined treatment the number of cycles increases to $N = 27\,500$.

The crack growth rate in the initial material is higher than for the material subjected to combined treatment: in the first case fracture occurs after $N = 3500$ cycles after the appearance of the crack, and in the second it occurs after $N = 5500$ cycles.

Noteworthy is that the crack growth rate in the specimen with the untreated welded joint (Fig. 6b) is inhomogeneous. The crack growth rate was estimated from optical micrographs of the surface, whereas the crack could be initiated in the bulk of the material due to structural macroheterogeneity of the weld. Taking into account this fact, the crack growth rate curve can change abruptly with a sharp variation in the value of the analyzed parameter. As for the specimen with the treated weld, the crack growth rate is much lower and smoothly increases with increasing number of loading cycles.

Figure 7 shows the distribution fields of the principal strain component ε_1 for specimens of both types obtained immediately before fracture. Note that cracks in the specimens were initiated in different regions. In the specimen with the untreated weld, the crack was initiated and grew from the flat front face of the specimen. In the specimen with the treated weld, the crack was initiated on the lateral face of the specimen and then emerged on the weld root surface. As one can see, the crack growth behavior is mainly brittle in the case with the untreated weld: there are no characteristic localized shear bands near the crack tip which are oriented in the directions of the maximum tangential stresses (Figs. 7a and 7b). In the case with the treated weld, a bud-like zone of developed plasticity is formed in the crack tip region (Fig. 7c), or the crack propagation is accompanied by localized shear banding (Fig. 7d).

The numerical characterization of the deformation behavior of both type specimens was carried out for an

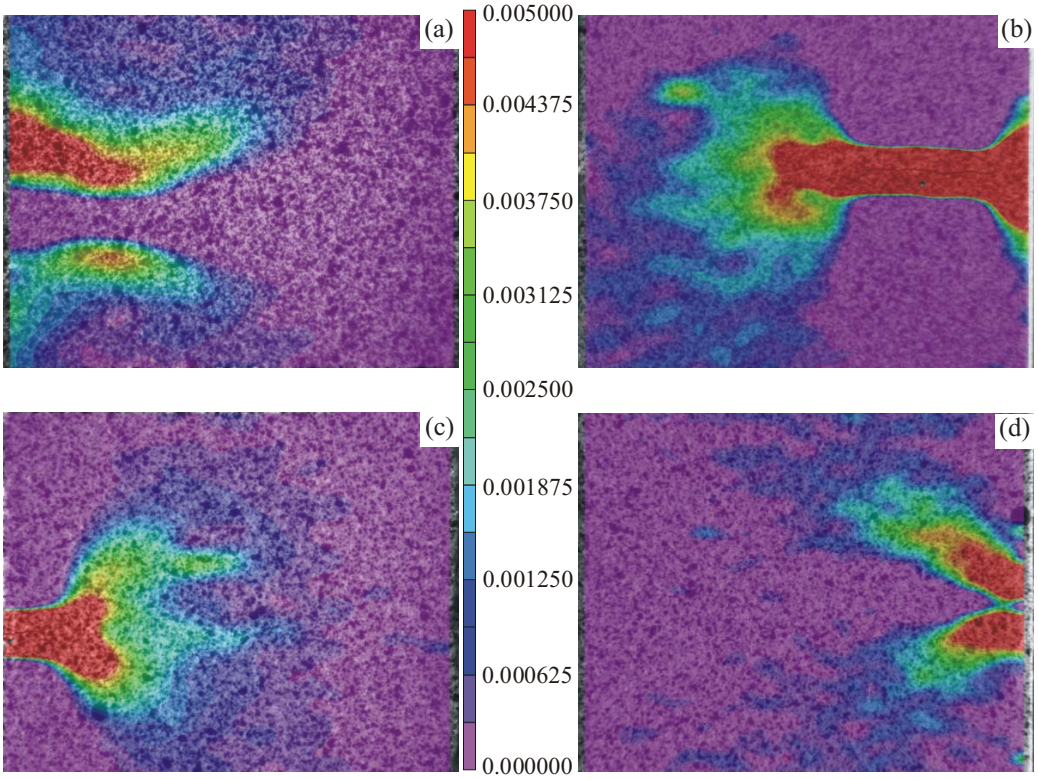

Fig. 7. Strain filed components ε_1 for the specimen with the untreated weld (a, b) and with the weld subjected to combined treatment (c, d), obtained on the front (weld face (a, c)) and back surface of the specimen (weld root (b, d)) (color online).

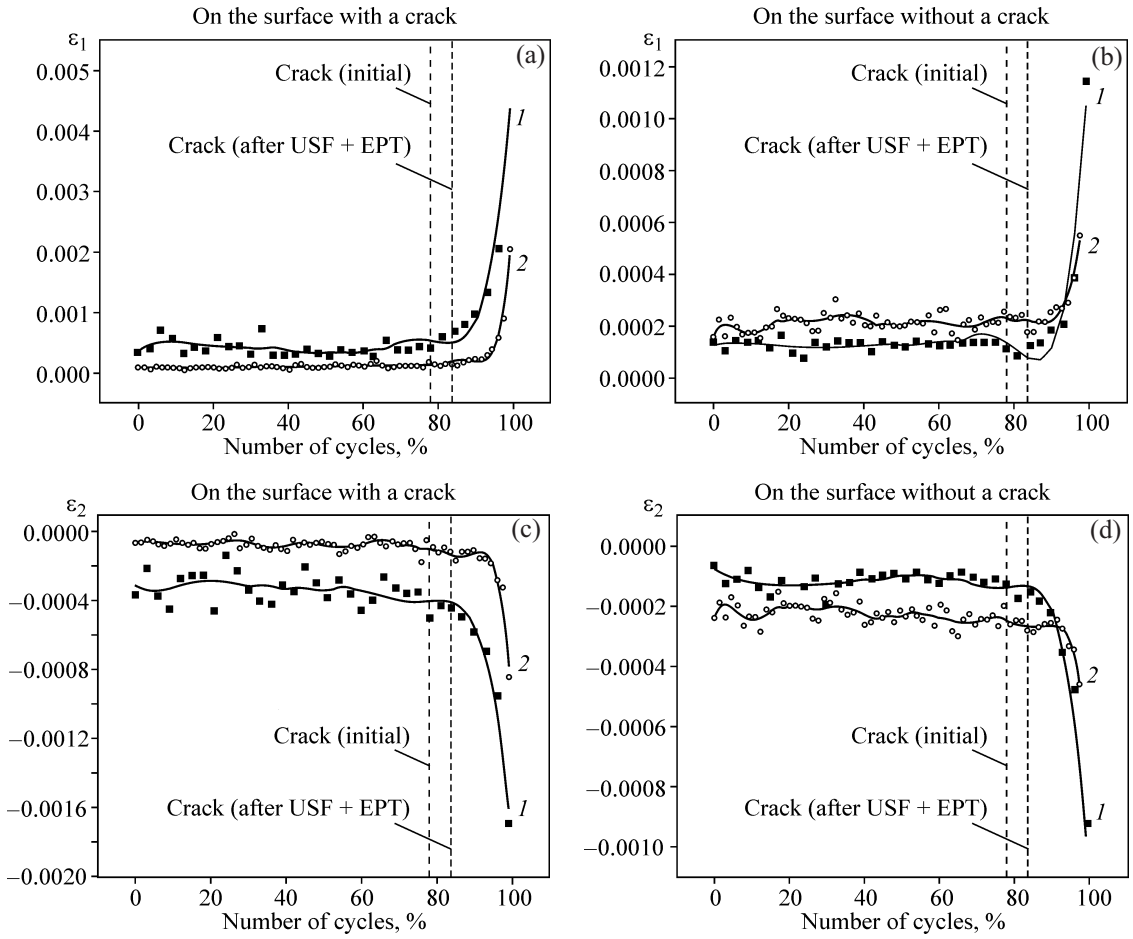

Fig. 8. Variation curves of the integral (averaged) value of the principal strain components ε_1 (a, b) and ε_2 (c, d) with increasing number of cycles for VT23 alloy specimens with the laser weld in the initial state (*1*) and subjected to ultrasonic forging (USF) with electric pulse treatment (EPT) (*2*) on the surface with a crack (a, c) and without a crack (b, d).

extracted square region of the image, with the width equal to the image one. The calculated principal strain values were averaged over this region; the estimation results are given in Fig. 8.

The plotted curves show that the strain component values remain almost constant during the test, but the value depends on the structural state of the specimen (untreated or subjected to the combined treatment) and on the point of observation. In general, the variation curves of both strain components ε_1 and ε_2 change in a similar way.

It can be seen that the observed cracking of the specimen with the untreated weld at an about 80% amount of cycles leads to a sharp increase in the average level of strain ε_1 on both sides of the specimen and to a decrease of ε_2. This means that the main crack propagates at a higher rate in the untreated specimen. Additionally, all the curves show that the catastrophic (avalanche) increase in the strain component values in specimens with the untreated weld begins earlier. Therefore we may conclude that the specimen with the treated welded joint is less sensitive to crack propagation.

4. DISCUSSION OF RESULTS

4.1. Fatigue Fracture of Materials as a Multilevel Nonlinear Process

It is well known [7–12] that a growing crack forms a system of successive grooves (so called striation) under low-cycle fatigue conditions. This means that there must be a critical number of crystal structure defects in the material in order for the fatigue crack to propagate under cyclic loading. The critical defect structure is phenomenologically introduced in all known models of fatigue crack growth mechanics [13–18, etc.]. For example, Murakami and Endo [14] established a power-law dependence of the threshold stress intensity factor on the defect size, $\Delta\kappa_{th} \sim l^{1/3}$. Their model is widely used in assessing the effect of small cracks, small holes, surface

roughness, nonmetallic inclusions, and other defects on the fatigue strength. Other models also employ the power-law dependence of the fatigue strength on the defect size, but the exponent is varied and the area of the defect is used instead of the linear defect size.

The necessity of taking into account defect interaction at the fatigue crack tip in fatigue crack growth models greatly complicates the modeling of fatigue failure. Therefore, we associate [19–22] fracture with the structural phase decomposition of the deformed crystal in the zones of high lattice curvature. Crack propagation is represented as a nonlinear wave process. Nonlinear fracture waves are dispersed in ductile fracture conditions, giving rise to local mesovortices in the form of dynamic rotations. Structural transformations in the zones of local lattice curvature ahead the crack tip are taken into account. A modified method of excitable cellular automata was developed to account for local force moments in the crystal lattice with broken translation invariance, and to calculate the work of rotational modes of deformation during crack growth. The multiscaling of structural scale levels of deformation during fracture of solids provides control over fracture processes in materials with different internal structures. Let us consider the structural scale levels of plastic deformation and fracture in the studied welded joints and their effect on the fatigue life of heterogeneous material.

4.2. Structural Scale Levels of Plastic Deformation in VT18U Alloy Weld after Ultrasonic Forging

The fatigue life of the VT18U alloy weld with a low content of the bcc β phase multiply increases due to ultrasonic forging. Ultrasonic forging causes high lattice curvature, formation of mesoscopic structural states in lattice interstitial sites, and plastic distortion of atoms from lattice sites to interstitial sites with the formation of nonequilibrium vacancies. The role of the motion of point defects in noncrystallographic plastic flow sharply increases and governs the nanoscale structural level of deformation, which was absent under cyclic loading of the initial welded joint. The interface between the weld root and the adjacent material is dispersed, and hence a through-the-thickness fatigue crack that breaks the specimen cannot be initiated at this interface.

Ultrasonic forging leads to surface layer nanostructuring, as is evident from Figs. 2b and 2c. The shear instability of nanograin boundaries associated with reversible transformations of their structure between the amorphous and nanocrystalline states determines high relaxation characteristics of the surface layer. This is a nanoscale structural level of deformation, which largely contributes to the increase in the fatigue life of the material under cyclic loading. Hence, since the nanostructured surface layer is adjacent to an elastically loaded underlying material that inhibits crack initiation in the nanocrystalline structure, the processing of the VT18U welded joints by ultrasonic forging proves to be very promising.

4.3. Structural Scale Levels of Plastic Deformation and Fracture of VT23 Alloy Weld Subjected to Ultrasonic Forging with High-Current Electric Pulse Treatment

The high concentration of the bcc β phase that contains vanadium, molybdenum, and chromium in the VT23 alloy makes it impossible to nanostructure the β phase by ultrasonic forging. However, a combination of ultrasonic forging and high-current electric pulse treatment allows the dispersion of β-phase bands by their longitudinal splitting, with the formation of α″ laths between the longitudinal subbands. A thermodynamically similar process was induced in Ti_3Al-based titanium alloys with the 10% Nb + 3% V + 1% Mo alloying elements that stabilize the bcc β phase [6]. High-temperature superplastic deformation of such alloys led to the growth of longitudinal hexagonal DO_{19} α_2' laths in β-phase bands. The superplasticity indicated a diffusion-controlled transformation of the bcc β phase into an hcp α_2' phase. Naturally, the diffusion-controlled structural phase transformation is impossible in the conditions of ultrasonic forging with electric pulse treatment. Therefore, the formation of α″ laths can occur by the mechanism of plastic distortion and within nanostructural configurations. The nanostructured boundaries of the β and α″ phases can be reversibly shifted under cyclic loading of the weld, leading to a twofold increase in the fatigue life of the VT23 alloy weld. This effect must be dependent on the electron beam treatment parameters.

Although the literature provides no unambiguous explanation of how high-current electric pulse treatment affects the plasticity of the material, we would offer our opinion according to the concept of Ref. [21]. Ultrasonic forging induces dynamic rotations in the material, which can strongly break the translation invariance of the crystal lattice. Valence electrons transfer to high energy states in the high lattice curvature zones in rotational clusters of the crystal lattice and form localized ion-electron clusters that fall out of the general electron energy spectrum of the translation-invariant crystal. This causes nano- or microcracking under ultrasonic forging. Electric pulse treatment pushes out localized high energy

electrons from rotational clusters. As a consequence, large localized clusters of positive ions in the crystal lattice are destroyed by the Coulomb inter action, and the shared electron energy spectrum characteristic of a translation-invariant lattice is restored. The transition of a part of binding d electrons of the β phase to the s-p states of the (Ti-Al) component in the alloy causes the formation of DO_{19} α″ laths. This is a nanoscale structural level of plastic deformation and fracture.

The above discussed nanostructural level of fracture is observed in the fracture micrographs of the VT23 welded joint subjected to ultrasonic forging with high-current pulsed electron beam treatment. It is observed as nanofibers formed in ductile fracture bands (Fig. 5d). The nanofibrous structure is formed by the dispersion of low-angle subboundaries in the lattice curvature zones [23]. However, only due to electric pulse treatment the fibrous structure of the subboundaries is dispersed into individual fibers that excite rotational modes of plastic flow during ductile fracture of the material. Some authors have already suggested that the precursor of ductile fracture is the formation of localized deformation bands and nanovoids [4]. However, the evolution mechanism of this precursor with crack initiation remains unclear. The experimental results in Fig. 5 indicate that fracture in the hierarchy from micro- to nanolevel is a multilevel process. The electronic subsystem creates mesoscopic structural states on the nanostructural level, which play an important role in the excitation of the rotational modes of fracture. The deformed material is fragmented with the formation of low-angle subboundaries that have a nanofibrous structure. The couple stresses associated with the rotational modes of deformation induce the dispersion of the nanofibrous structure of low-angle subboundaries with the formation of individual nanofibers and nanovoids. The dissipative nature of such processes makes for a decrease in the fatigue crack growth rate. This was convincingly showed in the experiment with the use of the digital image correlation method. The combination of ultrasonic forging with high-current electric pulse treatment offers multiple possibilities for the control over the formation of structural scale levels of deformation and fracture in heterogeneous media, which is important for increasing the fracture toughness of materials and their welds.

5. CONCLUSIONS

The processing of high-strength titanium alloy welds by ultrasonic forging or by its combination with high-current electric pulse treatment activates the micro- and nanoscale structural levels of plastic deformation and fracture. Such processing gives rise to lattice curvature in surface layers, formation of mesoscopic structural states in the interstitial sites of the curved lattice, plastic distortion, and a dramatic increase in the role of nonequilibrium point defects in plastic deformation and fracture of the material. With a low content of the bcc β phase in titanium alloy (VT18U), the most pronounced effects of ultrasonic forging are dispersion and nanostructuring of the surface layer, and a 4.6-fold increase in the fatigue life of welded joints. With a high bcc β phase content (laser welded alloy VT23), brittle welds exhibit plasticity and fatigue endurance only after a combined processing by ultrasonic forging and high-current electric pulse treatment. Nanoscale structural levels of deformation and fracture are observed as the growth of nanostructured α′ martensite (in the α phase) and α″ martensite (in the β phase). Fracture micrographs of the VT23 alloy welds demonstrate an alternation of cleavage bands and ductile fracture bands where nanofibers responsible for the excitation of the rotational modes of fracture are formed. In so doing, the fatigue crack growth rate decreases significantly.

ACKNOWLEDGMENTS

The work was carried out within the range of the TPU Competitiveness Enhancement Program (Project No. TPU CEP_IHTP_73\2017), as well as within the Fundamental Research Program of the State Academies of Sciences for 2013–2020 (Project III.23.1.1), RFBR Project No. 17-01-00691, and SB RAS Integration Project No. 4.

REFERENCES

1. Pleshanov, V.S., Kibitkin, V.V., and Panin, V.E., Mesomechanics of Fatigue Fracture for Polycrystals with Macroconcentrators, *Theor. Appl. Fract. Mech.*, 1998, vol. 30, no. 1, pp. 13–18. doi 10.1016/S0167-8442(98)00039-1
2. Khorev, A.I., Development of Titanium Sheet Alloys for Welded Structures Working at High Temperatures, *Welding Int.*, 2016, vol. 30, pp. 389–394.
3. Panin, V.E., Egorushkin, V.E., Elsukova, T.F., Surikova, N.S., Pochivalov, Y.I., and Panin, A.V., *Multiscale Translation-Rotation Plastic Flow in Polycrystals: Handbook of Mechanics of Materials*, Hsuch, C.-H. et al., Eds., Singapore: Springer Nature. doi 10.1007/978-981-10-6855-3_77-1
4. Tekoglu, C., Hutchinson, J.W., and Pardoen, T., On Localization and Void Coalescence as a Precursor to Duc-

tile Fracture, *Philos. Trans. R. Soc. A*, 2015, vol. 373, pp. 20140121.
5. Panin, V.E., Surikova, N.S., Smirnova, A.S., and Pochivalov, Yu.I., Mesoscopic Structural States under Plastic Deformation of Nanostructured Metallic Materials, *Phys. Mesomech.*, 2018, vol. 21, no. 5, pp. 396–400.
6. Yang, K.L., Huang, J.C., and Wang, Y.N., Phase Transformation in the β-Phase of Super α_2Ti_3Al Base Alloys during Static Annealing and Super Plastic Deformation at 700–1000°C, *Acta Mater.*, 2013, vol. 51, pp. 2577–2594.
7. Ivanova, V.S., *Synergetics: Strength and Fracture of Metallic Materials*, Cambridge: Cambridge International Science, 1998.
8. Ivanova, V.S. and Terentiev, V.F., *Fatigue of Metals*, Moscow: Metallurgiya, 1975.
9. Terentiev, V.F. and Korableva, S.A., *Fatigue of Metals*, Moscow: Nauka, 2015.
10. Makhutov, N.A., *Low-Cycle Fatigue*, Moscow: Mashinostroenie, 2010, pp. 217–285.
11. Shanyavsky, A.A., *Simulation of Fatigue Fracture of Metals. Synergetics in Aviation*, Ufa: Monografiya, 2007.
12. Shanyavsky, A.A., Scales of Metal Fatigue Cracking, *Phys. Mesomech.*, 2015, vol. 18, no. 2, pp. 163–173.
13. Frost, N.E., Marsh, K.J., and Pook, L.P., *Metal Fatigue*, Oxford: Oxford Univ. Press, 1974.
14. Murakami, Y. and Endo, M., Effect of Defects, Inclusions and Inhomogeneities on Fatigue Strength, *Int. J. Fatigue*, 1994, vol. 16, pp. 163–182.
15. Botvina, L.R., *Fracture: Kinetics, Mechanisms, General Laws*, Moscow: Nauka, 2008.
16. Barenblatt, G.I. and Botvina, L.R., Self-Similarity of Fatigue Fracture: Damage Accumulation, *Izv. AN SSSR, Mekh. Tverd. Tela*, 1983, no. 44, pp. 161–165.
17. Botvina, L.R. and Barenblatt, G.I., Self-Similarity of Damage Accumulation, *Probl. Prochn.*, 1985, no. 12, pp. 17–24.
18. Barenblatt, G.I., Scaling Phenomena in Fatigue and Fracture, *Int. J. Fract.*, 2006, vol. 138, pp. 19–35.
19. Egorushkin, V.E., The Gauge Dynamic Theory of Defects in Structured Media under Inhomogeneous Deformation, *Izv. Vuz. Fiz.*, 1990, vol. 33, no. 2, pp. 51−68.
20. Moiseenko, D.D. and Panin, V.E., Physical Fracture Mesomechanics of Solids Treated as Nonlinear Hierarchically Organized Systems, *Mech. Solids*, 2015, vol. 50, no. 4, pp. 400–411.
21. Egorushkin, V.E., Panin, V.E., and Panin, A.V., Lattice Curvature, Shear Bands, and Electroplastic Effect, *Phys. Mesomech.*, 2018, vol. 21, no. 5, pp. 390–395.
22. Panin, V.E., Fracture Mechanisms of a Solid as a Nonlinear Hierarchically Organized System, *Proc. Eur. Conf. Fracture 19, Kazan, Russia, 2012*, Kazan: Kazan Sci. Center RAS, 2012.
23. Panin, V.E., Egorushkin, V.E., Surikova, N.S., and Pochivalov, Yu.I., Shear Bands as Translation-Rotation Mode of Plastic Deformation in Solids under Alternate Bending, *Mater. Sci. Eng. A*, 2017, vol. 703, pp. 451–460.